AD-A033 202 HAWAII INST OF GEOPHYSICS HONOLULU F/G 8/5
THE EFFECT OF SEAMOUNTS AND OTHER BOTTOM TOPOGRAPHY ON MARINE G--ETC(U)
1974 J C ROSE, B R BOWMAN N00014-70-A-0016-0001
UNCLASSIFIED HIG-CONTRIB-608 NL

| OF |
AD
A033202

END

DATE
FILMED
2-77

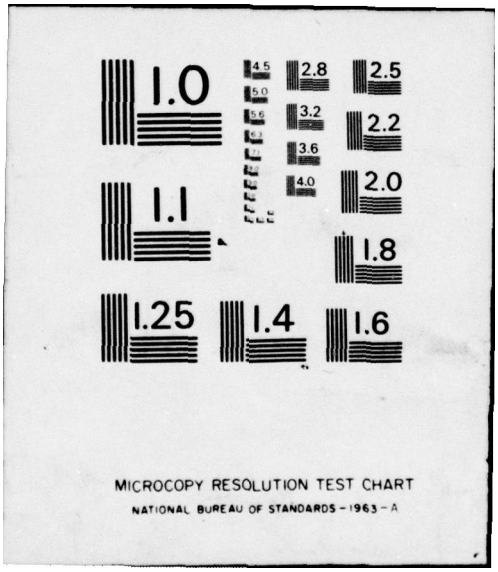
1.0
1.1
1.25
1.4
1.6
1.8
2.0
2.2
2.5
2.8
3.2
3.6
4.0
4.5
5.0
5.6
MICROCOPY RESOLUTION TEST CHART
NATIONAL BUREAU OF STANDARDS - 1963 - A

Unclassified

SECURITY CLASSIFICATION OF THIS PAGE (When Data Entered)

(12)

REPORT DOCUMENTATION PAGE

READ INSTRUCTIONS BEFORE COMPLETING FORM

1. REPORT NUMBER (14) HIG-Contribution-608	2. GOVT ACCESSION NO.
3. RECIPIENT'S CATALOG NUMBER	
4. TITLE (and Subtitle) (6) THE EFFECT OF SEAMOUNTS AND OTHER BOTTOM TOPOGRAPHY ON MARINE GRAVITY ANOMALIES	5. TYPE OF REPORT & PERIOD COVERED
6. PERFORMING ORG. REPORT NUMBER HIG-Contribution 608	
7. AUTHOR(s) John C. Rose and Bruce R. Bowman (10)	8. CONTRACT OR GRANT NUMBER(s) (15) N00014-70-A-0016-0001
9. PERFORMING ORGANIZATION NAME AND ADDRESS Hawaii Institute of Geophysics 2525 Correa Road Honolulu, HI 96822	10. PROGRAM ELEMENT, PROJECT, TASK AREA & WORK UNIT NUMBERS (12) 18 p.
11. CONTROLLING OFFICE NAME AND ADDRESS Office of Naval Research Ocean Science & Technology Division Arlington, VA 22217	12. REPORT DATE (11) 1974
	13. NUMBER OF PAGES -16-
14. MONITORING AGENCY NAME & ADDRESS(if different from Controlling Office) Office of Naval Research Branch Office 1030 East Green Street Pasadena, CA 91106	15. SECURITY CLASS. (of this report) Unclassified
	15a. DECLASSIFICATION/DOWNGRADING SCHEDULE

16. DISTRIBUTION STATEMENT (of this Report)

Approved for public release; distribution unlimited.

DDC DEC 8 1976 RECEIVED

17. DISTRIBUTION STATEMENT (of the abstract entered in Block 20, if different from Report)

18. SUPPLEMENTARY NOTES

Published in Proceedings of the International Symposium on Applications of Marine Geodesy, p. 381-396, Marine Technology Society, Washington, D. C. 1974.

19. KEY WORDS (Continue on reverse side if necessary and identify by block number)

Marine gravity
Bottom topography
Seamounts
Solid angle elliptic integrals
Gravity effect of seamounts

20. ABSTRACT (Continue on reverse side if necessary and identify by block number)

Localized bathymetric features produce large amplitude perturbations in the marine free-air gravity anomalies. In order to study long wavelength anomalies, which are of particular interest in marine geodesy, it is desirable to remove the topography "noise level". However, to do this in a truly three-dimensional fashion along a marine gravity track is not practical because of the formidable amount of data preparation required. It is also undesirable to use conventional Bouguer anomalies because these can easily be in error by 60% because of the one-dimensional nature of the correction.

CONT on next page

DD FORM 1 JAN 73 1473 EDITION OF 1 NOV 65 IS OBSOLETE S/N 0102-014-6601 | (cont.)

Unclassified

SECURITY CLASSIFICATION OF THIS PAGE (When Data Entered)

164 400 mt

20. Abstract (cont.)

We have developed a computer program which calculates the sea-surface three-dimensional gravity effect of a conical seamount from a point above the apex to any distance off-axis. The results of this program are compared with those of a Talwani two-dimensional equivalent of a ship track across the off-axis hyperbolic slice of the cone. A study of more than 100 seamounts in the Pacific Ocean showed that their slope angles range from 4.5° to 17°. For this reason, model cases with slope angles of 5°, 10° and 15° in water depths of 1 to 6 km were considered. For a seamount with its apex at 2-km depth and base at 5-km depth and 10° slope angle, the two-dimensional method overcorrects by 18% over the apex, but gives the same result as the three-dimensional method at an off-axis distance of 60% of the base radius. Farther out than 60% of the base radius, the two-dimensional method undercorrects. We have developed a second computer program which uses a two-dimensional method to correct the free-air anomaly for topography along the ship's track. Curves from the cone program as well as two-dimensional topography corrected free-air anomaly tracks are presented.

THE EFFECT OF SEAMOUNTS AND OTHER BOTTOM TOPOGRAPHY ON MARINE GRAVITY ANOMALIES

John C. Rose
Hawaii Institute of Geophysics
University of Hawaii
Honolulu, Hawaii 96822

Bruce R. Bowman
Hawaii Institute of Geophysics
University of Hawaii
Honolulu, Hawaii 96822

ABSTRACT

Localized bathymetric features produce large amplitude perturbations in the marine free-air gravity anomalies. In order to study long wavelength anomalies, which are of particular interest in marine geodesy, it is desirable to remove the topography "noise level". However, to do this in a truly three-dimensional fashion along a marine gravity track is not practical because of the formidable amount of data preparation required. It is also undesirable to use conventional Bouguer anomalies because these can easily be in error by 60% because of the one-dimensional nature of the correction. We have developed a computer program which calculates the sea-surface three-dimensional gravity effect of a conical seamount from a point above the apex to any distance off-axis. The results of this program are compared with those of a Talwani two-dimensional equivalent of a ship track across the off-axis hyperbolic slice of the cone. A study of more than 100 seamounts in the Pacific Ocean showed that their slope angles range from 4.5° to 17°. For this reason, model cases with slope angles of 5, 10 and 15 in water depths of 1 to 6 km were considered. For a seamount with its apex at 2 km depth and base at 5 km depth a 10° slope angle, the two-dimensional method over-corrects by 18% over the apex, but gives the same result as the three-dimensional method at an off-axis distance of 60% of the base radius. Farther out than 60% of the base radius, the two-dimensional method under-corrects. We have developed a second computer program which uses a two-dimensional method to correct the free-air anomaly for topography along the ship's track. Curves from the cone program as well as two-dimensional topography corrected free-air anomaly tracks are presented.

INTRODUCTION

Gravity anomaly data, particularly in the form of 1°x1° means, are needed in order to determine undulutions of the gravimetric geoid, determine components of the deflection of the vertical, and to derive an earth gravity model, i.e., a spherical harmonic expression of gravity variations on a global basis.

In continental areas, good approximations of mean 1°x1° can be made in most areas. Part of the reason for this is that land gravity measurements can be made at relatively low cost for quite

a large number of stations. Any station location is well know, and the gravimeter is stationary during the observation. Many areas of large extent have observations on a grid-like pattern, and there are enough point anomalies available so that simple averaging can be done and a reliable mean is obtained. Good topographic maps are available so that terrain corrections can be made.

The situation is not so good as regards marine gravity results. One factor is the high cost of the sea gravimeter itself, at least 15 times the cost of land meter. Another is the very high cost of ship operation. A ship suitable for sea-gravity observations costs thousands of dollars a day to operate. These two factors alone indicate not only why there are great gaps in the sea gravity data, but also why the areal coverage usually consists of a long single track through a region rather than a grid pattern of observations. Then it becomes much more difficult with the sea data to determine mean 1°x1° anomalies than it has been for the land data. To make matters worse, the ocean bottom very often has relatively high relief which usually consists of seamounts. Because of navigation uncertainties, the exact location as well as configuration of bottom topography is not well know. In addition, slope corrections to the echo sounder depths have probably not been made, so that in bottom topography configurations where there is a high slope angle, the charted depths may be incorrect. In this regard see Krause (1962).

For land gravity observations, a several km high topographic feature only a few kilometers away has virtually no terrain effect on the vertical component of gravity. At sea, however, the observation point, instead of being at almost a right angle to the feature, is usually above the level of the top of the feature. Therefore the angle from the observation point to the center of mass of the topographic feature will be considerably different from nearly horizontal, and the gravity effect much larger.

It is well known that marine gravity results are only as good as the cross-coupling corrections, horizontal acceleration corrections, and Eotvos corrections. These matters will not be discussed in this paper. The problem which we want to examine here is that of effectively removing the "noise-level" or perturbations in the free-air anomaly, caused by the bottom topography, to obtain a residual gravity field which incorporates only the effect of the deeper mass distributions. The situation is the inverse of the one encountered by the paleomagnetic investigators where they remove the regional so that they can look at the local effects. The most difficult topography effect to remove is one that is truly three-dimensional; one of the most common features in marine bottom topography is the submerged seamount. We thought that it would be profitable to study the difference between the three-dimensional (3D), two-dimensional (2D) and one-dimensional (1D) gravity effect of conical seamounts.

THE GRAVITY EFFECT OF A CONICAL SEAMOUNT

We felt that it was reasonable to assume that the form of a submerged seamount could be approximated as a perfect cone, although we realized that no such seamount probably exists. Our chief purpose in addition to producing a table of gravity effects was to compare one and two-dimensional approximations with the three-dimensionally derived gravity effects. We examined the bathymetry character of more than 100 "reasonable" seamounts in the central Pacific Ocean. The slope angles were calculated from the height divided by base radius, and were found to range from 4.5 to 17 degrees with 10 degrees as a reasonable mean. Appendix A gives a summary of the developments leading to a group of equations used for calculating the off axis vertical gravity

effect of a horizontal circular disk. The seamount was then approximated from stacking up to 100 varying sized disks. We used a density of 2.3 g/cc*, or a differential density of (2.3-1.027) g/cc.

Tables 1, 2 and 3 give the vertical gravitional attraction of conical seamounts of density 2.3 g/cc and having slopes of 5, 10 and 15 degrees respectively. The tables give the radial distance in km from the axis corresponding to an even 10 mgal unit. For cases where the on-axis mgal effect is not an even 10 mgal unit, the mgal effect is given in parentheses in place of the zero-km number. The purpose in presenting the tables in this form is to permit other investigators to construct graphs of their own to any scale. Drawn as plan view circles at the appropriate radii, they would permit the gravity effect profile of an off-axis ship track to be determined. If some other density ρ besides 2.3 is desired, multiply the mgal effect by $(\rho - 1.027)/(2.3-1.027)$.

The 3-dimensional results were compared not only with Talwani, et. al. (1959) 2D equivalents of ship tracks across off-axis slices of the cone, but also with 1D corresponding approximations along each track. The ship track distance increments were 5 km, because this is about the distance a ship will travel in 15 minutes at 10.5 knots, and our ship gravity results are given for even quarter hour times. Table 4 presents the comparisons for the on-axis ship track cases. In order to discuss off-axis cases, it seemed best to pick a few examples of reasonable situations encountered at sea. Figure 1 shows a half-profile of the vertical gravity effect of 10° as well as 15° conical seamounts where the base depth is 5 km and the depth to the top is one km. Figure 2 shows the mgal error in using a 1D

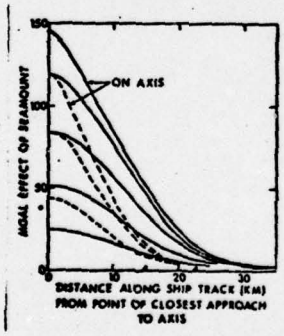

Figure 1. Vertical gravity effect at sea-level of two conical seamounts. Both have a base depth of 5 km and a top depth of 1 km. Solid lines are for one with a 10° slope from the horizontal, and dashed lines are for one with a 15° slope. Corresponding base radii are indicated by the open triangles. Effects are shown along ship tracks crossing on-axis, as well as flank crossings at 5 km successive offsets from the axis.

*In 1971, R/V KANA KEOKI with LaCoste and Romberg gravimeter S33 crossed the Necker Ridge. Furumoto, et. al. (1971) had established a reversed refraction seismic line located 100 km east of the axis of the ridge and 100 km northeast of the gravity profile. The km thickness and km/sec seismic velocity values of the upper three layers of the sea floor (0.1, 2.3; 0.3, 2.9; 1.8, 3.6) along with the Ludwig, Nafe and Drake (1970) corresponding densities of 2.06, 2.21 and 2.33 g/cc yield a mean density of 2.30 g/cc. A Talwani (1959) 2D density profile was used, and 2.30 was confirmed as the best density to use. This agrees with conclusions of Woollard (1951) and to some extent with those of Strange, et al. (1965).

TABLE 1. Sea level mgal effect and corresponding distance from axis in kilometers for seamounts with a slope of 5 degrees and density 2.3 g/cc.

DEPTH OF BASE (KM)		6						5					4				3			2		1
DEPTH OF TOP (KM)		0	1	2	3	4	5	0	1	2	3	4	0	1	2	3	0	1	2	0	1	0
	300	(292)						ON AXIS MGAIS IN PARENTHESES (0 KM)														
		0.5																				
		2.7																				
		4.9																				
		7.1																				
	250	9.2						(244)														
		11.5						0.7														
		13.7	(223)					3.0														
		15.9	1.6					5.1														
		18.2	4.7					7.3														
	200	20.4	7.3					9.6					(195)									
		22.7	9.8					11.8					1.1									
		24.9	12.2					14.0	(175)				3.2									
		27.2	14.7	(161)				16.3	2.4				5.4									
		29.5	17.1	1.3				18.5	5.3				7.6									
	150	31.9	19.5	5.4				20.8	7.9				9.9				(146)					
		34.2	21.9	8.4				23.1	10.4				12.1				1.3					
		36.6	24.3	11.2				25.4	12.9				14.4	(127)			3.5					
		38.9	26.8	13.9				27.7	15.3	(115)			16.6	3.3			5.7					
		41.3	29.2	16.5	(105)			30.1	17.8	3.3			18.9	6.0			8.0					
	100	43.8	31.7	19.1	3.9			32.5	20.2	6.7			21.2	8.6			10.2			(97)		
		46.2	34.2	21.8	7.7			34.9	22.7	9.6			23.6	11.1			12.5	(81)		1.6		
		48.7	36.8	24.4	10.9			37.3	25.2	12.4			26.0	13.6			14.8	0.5		3.8		
		51.3	39.4	27.1	14.0			39.8	27.8	15.1	(62)		28.4	16.2	0		17.1	4.2		6.1		
		53.9	42.0	29.8	17.0	0		42.3	30.3	17.9	2.2		30.8	18.7	5.1		19.5	6.7		8.3		
	50	56.6	44.7	32.6	20.0	4.6		44.9	33.0	20.7	6.8		33.3	21.3	8.3		21.9	9.6		10.6		(49)
		59.5	47.6	35.5	23.0	9.0		42.7	35.8	23.5	10.3		36.0	24.0	11.3		24.4	12.2		13.0	(35)	1.9
		62.6	50.7	38.7	26.3	12.9		50.6	38.7	26.6	13.7		38.7	26.8	14.3	(22)	27.0	14.9	(27)	15.4	2.6	4.2
		66.2	54.3	42.3	29.9	16.9	0	53.9	42.0	29.9	17.2	(18)	41.7	29.8	17.5	2.6	29.7	17.8	4.5	18.0	5.7	6.5
	10	72.2	59.9	47.6	34.9	21.8	6.4	58.8	46.6	34.3	21.6	7.3	45.8	33.7	21.4	7.9	33.1	21.1	8.4	20.9	8.8	9.0
	5	80.0	67.0	53.7	40.1	26.0	10.7	64.8	51.9	38.8	25.4	10.9	50.1	37.5	24.6	10.9	36.1	23.1	10.9	22.9	10.7	10.5
	1	109.9	97.0	78.5	59.4	39.8	19.3	91.4	74.1	56.3	37.8	18.5	69.1	52.7	35.5	17.6	48.4	32.8	16.5	29.5	15.0	13.0

MGAIS

KILOMETERS FROM AXIS

TABLE 2. Sea level mgal effect and corresponding distance from axis in kilometers for seamounts with a slope of 10 degrees and density 2.3 g/cc.

DEPTH OF BASE (KM)		6						5					4				3			2		1
DEPTH OF TOP (KM)		0	1	2	3	4	5	0	1	2	3	4	0	1	2	3	0	1	2	0	1	0
	270	(265)																				
		0.5						ON AXIS MGAIS IN PARENTHESES (0 KM)														
	250	1.7																				
		2.8																				
		3.9						(221)														
		5.1						0.1														
		6.2						1.2														
	200	7.3						2.3														
		8.5	(187)					3.4														
		9.8	2.0					4.6					(176)									
		11.0	3.7					5.8					0.7									
		12.2	5.2					7.0					1.8									
	150	13.5	6.6					8.2	(145)				3.0									
		14.7	8.0					9.4	1.6				4.2				(132)					
		16.0	9.4	(125)				10.6	3.4				5.3				0.3					
		17.3	10.7	2.3				11.9	4.9				6.5				1.4					
		18.6	12.1	4.5				13.1	6.3				7.7	(103)			2.5					
	100	20.0	13.7	6.3				14.4	7.8				9.0	1.2			3.7					
		21.4	15.0	8.0				15.8	9.2	(86)			10.2	3.1			4.9			(88)		
		22.8	16.5	9.6	(73)			17.1	10.7	2.6			11.5	4.7			6.1			0.9		
		24.1	18.0	11.3	2.3			18.5	12.2	4.8			12.9	6.2			7.4	(63)		2.1		
		25.9	19.6	13.0	5.2			20.0	13.7	6.6			14.3	7.8			8.7	1.1		3.3		
	50	27.5	21.3	14.8	7.4			21.6	15.3	8.5			15.7	9.3	(49)		10.0	3.1		4.5		(44)
		29.3	23.2	16.7	9.6	(32)		23.2	17.0	10.3	(39)		17.3	10.9	3.4		11.4	4.8		5.8		0.5
		31.5	25.2	18.8	11.9	2.4		25.1	18.9	12.3	4.5		18.9	12.7	5.7		12.9	6.5		7.2	(24)	1.6
		34.1	27.9	21.4	14.5	6.5		27.5	21.2	14.7	7.4		21.0	14.7	7.9	(11)	14.7	8.4	(16)	8.6	1.7	2.9
	10	39.0	32.4	25.5	18.4	10.6	(6)	31.4	24.8	18.0	10.8	(8)	24.0	17.6	10.8	1.8	17.1	10.7	3.3	10.5	4.0	4.3
	5	45.3	37.9	30.3	22.4	14.0	3.2	36.2	29.0	21.6	13.8	4.3	27.6	20.6	13.3	4.9	19.5	12.8	5.3	12.0	5.4	5.3
	1	69.0	58.3	47.2	35.7	23.7	10.8	54.6	44.3	33.6	22.5	10.5	41.0	31.3	21.1	10.1	28.5	19.3	9.5	17.1	8.7	7.3

MGAIS

KILOMETERS FROM AXIS

Rose and Bowman

Table 3. Sea level mgal effect and corresponding distance from axis in kilometers for seamounts with a slope of 15 degrees and density 2.3 g/cc.

DEPTH OF BASE (KM)		6						5					4				3			2		1
DEPTH OF TOP (KM)		0	1	2	3	4	5	0	1	2	3	4	0	1	2	3	0	1	2	0	1	0
MGAL	240	(237)	ON AXIS MGALS IN PARENTHESES (0 KM)																			
		0.6																				
		1.4																				
		2.2																				
	200	3.0						(198)														
		3.8						0.6														
		4.6						1.4														
		5.5						2.2														
		6.3	(156)					3.0					(158)									
	150	7.2	1.5					3.9					0.6									
		8.1	2.9					4.7					1.4									
		9.0	4.0					5.6					2.3									
		10.0	5.1					6.5	(119)				3.1				(119)					
		11.0	6.2					7.4	2.0				3.9				0.7					
	100	11.9	7.3	(98)				8.3	3.3				4.8				1.5					
		13.0	8.4	2.5				9.3	4.5				5.7	(83)			2.3					
		14.1	9.6	4.2				10.3	5.6				6.6	1.1			3.2			(79)		
		15.2	10.7	5.6				11.4	6.8	(65)			7.6	2.6			4.1			0.7		
		16.4	12.0	7.1	(52)			12.5	8.0	2.0			8.7	3.9			5.0			1.6		
	50	17.7	13.3	8.6	1.6			13.7	9.2	3.9			9.7	5.1			6.0	(49)		2.4		
		19.1	14.8	10.1	4.4			15.0	10.6	5.6			10.9	5.4	(35)		7.0	2.1		3.3		0
		20.9	16.5	11.9	6.6			16.5	12.1	7.3	(26)		12.3	7.8	2.1		8.2	3.5		4.3		0.8
		23.2	18.8	14.1	9.0	0		18.5	14.1	9.3	3.3		13.9	9.5	4.4		9.6	5.1		5.5	(17)	1.7
	10	27.4	22.6	17.7	12.4	6.2		21.9	17.1	12.3	6.7		16.6	12.0	7.0	(6)	11.6	7.1	0	7.0	2.2	2.8
	5	32.6	27.2	21.6	15.8	9.4	(3)	25.9	20.7	15.3	9.4	(4)	19.6	14.6	9.2	2.1	13.7	8.9	3.1	8.3	3.5	3.6
	1	51.4	43.4	35.1	26.5	17.3	7.0	40.5	32.8	25.0	16.5	7.3	30.3	23.1	15.4	7.1	20.9	14.0	6.8	12.5	6.3	5.3

KILOMETERS FROM AXIS

flat-slab assumption (upper graph) in correcting to the 5 km base level, as well as the mgal error using a 2D Talwani method along the track. It is apparent that, on the axis, the 1D error is enormous, being 48% too large, while the 2D is much more reasonable at 16% too large. On axis, the 1D as well as 2D methods are blind to the deficiency of mass laterally. For the 10° seamount and 1D assumption, a conventional marine Bouguer anomaly, in which the sea water is replaced by rock, would over-correct the 145 mgal free-air anomaly by 69 mgal and appear as a large negative spike of almost half the amplitude of the original anomaly. Clearly, then, the 2D assumption is much better because in the worst case (on-axis), the 145 mgal free-air anomaly would be reduced to only -23 mgal, and at 10 km off-axis, to -8 mgal. The 2D-3D graphs for cases other than that shown in Figure 2 are quite similar in shape, and all exhibit the equality of 2D with 3D methods when the off-axis trackline distance is about 60 to 70 percent of the base radius. This percentage is given in the % RAD 2D = 3D column in Table 4. Of course, the 2D assumption under-corrects for topography when the off-axis distance is too great.

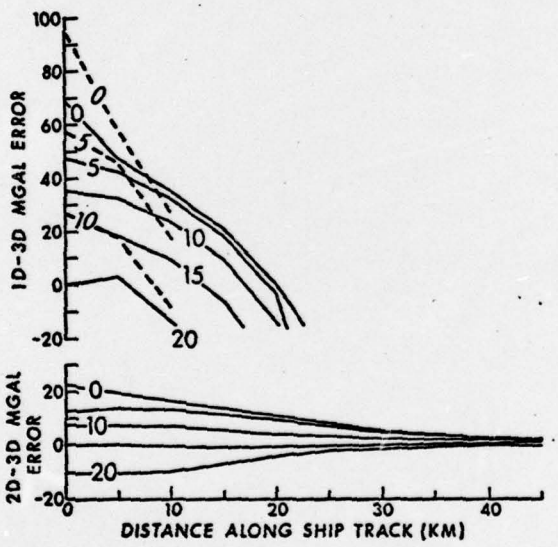

Figure 2. Mgal errors of 1D (upper) and 2D (lower) assumptions relative to the curves shown in Fig. 1. Only the 10° case is shown in the 2D-3D graph. Insert numbers give km offsets from the axis.

EFFECT OF FEATURES OFF THE TRACKLINE

It is important to know th magnitude of the gravity effect of features off to the side of the trackline and not seen directly by the echo-sounding device on the ship. The half-angle of a conventional echo-sounder cone of energy is 30° relative to the vertical. This means that the echo-sounder's lateral effectiveness ranges from 3.5 km in 6 km of water to 1.7 km in 3 km of water. From the base radii given in Table 4 it is seen that for all cases given in Tables 1, 2 and 3, the worst error encountered in ignoring seamounts off to the side of the track is 13 mgal for a 15° slope at zero km to the top and 6 km base depth. Almost all other cases are 10 mgal or less. The validity of ignoring lateral topography would not be true, however, if there were a large 2D bathymetric feature parallel to the trackline but just out of range the echo-sounder. Thus

TABLE 4. The vertical gravitational attraction, at sea level and on the axis, of a seamount, and the comparison with one as well as two-dimensional approximations. Density is 2.3 g/cc.

KM TO TOP	KM TO BASE	5° SLOPE BASE KM RADIUS	3D MGAL	1D-3D MGAL	2D-3D MGAL	% RAD. 2D=3D	10° SLOPE BASE KM RADIUS	3D MGAL	1D-3D MGAL	2D-3D MGAL	% RAD. 2D=3D	15° SLOPE BASE KM RADIUS	3D MGAL	1D-3D MGAL	2D-3D MGAL	% RAD. 2D=3D
0	6	68.6	292	28	10	74	34.0	265	55	20	71	22.4	237	83	30	68
1	6	57.2	223	44	15	71	28.4	187	80	27	67	18.7	156	111	36	64
2	6	45.7	161	53	17	68	22.7	125	89	27	66	14.9	98	116	33	63
3	6	34.3	105	55	17	65	17.0	73	87	25	63	11.2	52	108	29	62
4	6	22.9	55	52	14	63	11.3	32	75	19	62	7.5	20	87	21	63
5	6	11.4	15	38	10	63	5.7	6	47	10	66	3.7	3	50	10	--
0	5	57.2	244	23	9	73	28.4	221	47	17	71	18.7	198	69	25	65
1	5	45.7	175	39	13	70	22.7	145	69	23	66	14.9	119	95	30	63
2	5	34.3	115	45	14	67	17.0	86	74	22	63	11.2	65	95	27	60
3	5	22.9	62	45	13	63	11.3	39	68	18	59	7.5	26	81	21	60
4	5	11.4	18	35	9	70	5.7	8	45	10	70	3.7	4	49	12	--
0	4	45.7	195	19	7	73	22.7	176	38	13	69	14.9	158	56	20	65
1	4	34.3	127	33	11	68	17.0	103	57	18	64	11.2	83	77	24	60
2	4	22.9	70	37	11	65	11.3	49	58	17	58	7.5	35	72	20	58
3	4	11.4	22	31	5	59	5.7	11	42	10	65	3.7	6	47	14	--
0	3	34.3	146	14	5	65	17.0	132	28	10	65	11.2	119	41	15	58
1	3	22.9	81	26	8	66	11.3	63	44	14	56	7.5	49	58	18	57
2	3	11.4	27	26	8	56	5.7	16	37	10	65	3.7	10	43	14	--
0	2	22.9	97	10	4	76	11.3	88	19	7	56	7.5	79	28	11	54
1	2	11.4	35	18	6	52	5.7	24	29	9	65	3.7	17	136	14	--
0	1	11.4	49	4	2	51	5.7	44	9	4	58	3.7	40	13	7	--

scraps, trenches, ridges, island chains and continental slopes, for example could not be ignored. However, such situations would be treated as special cases.

MOVING WINDOW TOPOGRAPHY CORRECTION

We have developed a computer program which we call TCFAA (Topography Corrected Free Air Anomaly). Its purpose is to be a relatively inexpensive method of correcting the marine observed free-air anomalies for the effect of bottom topography along the track. A "boxcar window" is centered on the observation point. The mean water depth, maximum water depth, and mean free-air anomaly are calculated for only the sequence of track data within the window. The Talwani 2D effect of the topography relative to the mean depth is calculated and subtracted from the free-air anomaly. Except for discrepancies between the 2D assumption and 3D configurations, the result approximates a "complete" free air anomaly relative to the mean depth for the window. The window is advanced along the track along with each new observation point.

The results of a test of the program are shown in Figure 3. The track was taken from Leg 8 of KANA KEOKI in 1973 and goes from 5.5°S 168°W (left) to 3°S 175.5°W (right). All bathymetric "bumps" are crossings of essentially conical seamounts. The center of the track is about 120 km south of Canton Island and the bathymetric depression past 800 km is a western extension of the Nova Canton Trough and is therefore two-dimensional. Figure 3a shows original data. Figure 3b shows the results of using a window width of 110 km corresponding to 1°, and Figure 3c shows the results of using a window width of 330 km corresponding to 3° geographically.

DISCUSSION OF RESULTS

Figure 3b shows a very close correspondence between the mean free-air anomaly and TCFAA. This would be expected because TCFAA is done relative to the mean water depth. Over 1° or 110 km the area should be only 50 percent isostatically compensated, as has been pointed out by Woollard (1962). Because the lateral effect of seamounts not seen by the echo-sounder can be effectively ignored, we feel that the mean topography and free-air anomalies obtained with a 110 km window and a single ship track should provide powerful information for determining a local area basic predictor. This, in turn, can be used to determine the local 1°x1° mean anomaly. The TCFAA profile for a 110 km window probably cannot be used profitably for geological structure interpretation. This is because the mean water depth does not truly represent the most commonly occurring water depth for the whole region in general. The most common depth would be given by the "mode," which might not be possible to find in cases of a monocline or sawtooth topography, for example. There is a way out of this problem, however. Woollard (1962) maintained that topographic features must be about 3°x3° or larger in order to be compensated more than 80%. This is the reason we also show results obtained with a 330 km window.

Figure 3c shows that the TCFAA from a 330 km window should be very useful for local crustal structure interpretations. In particular, the departures of TCFAA from the 330 km mean free-area anomaly indicate areas of probably structural or tectonic interest. The mean free-air anomaly as well as mean topography change very slowly and would be quite useful for a regional basic predictor.

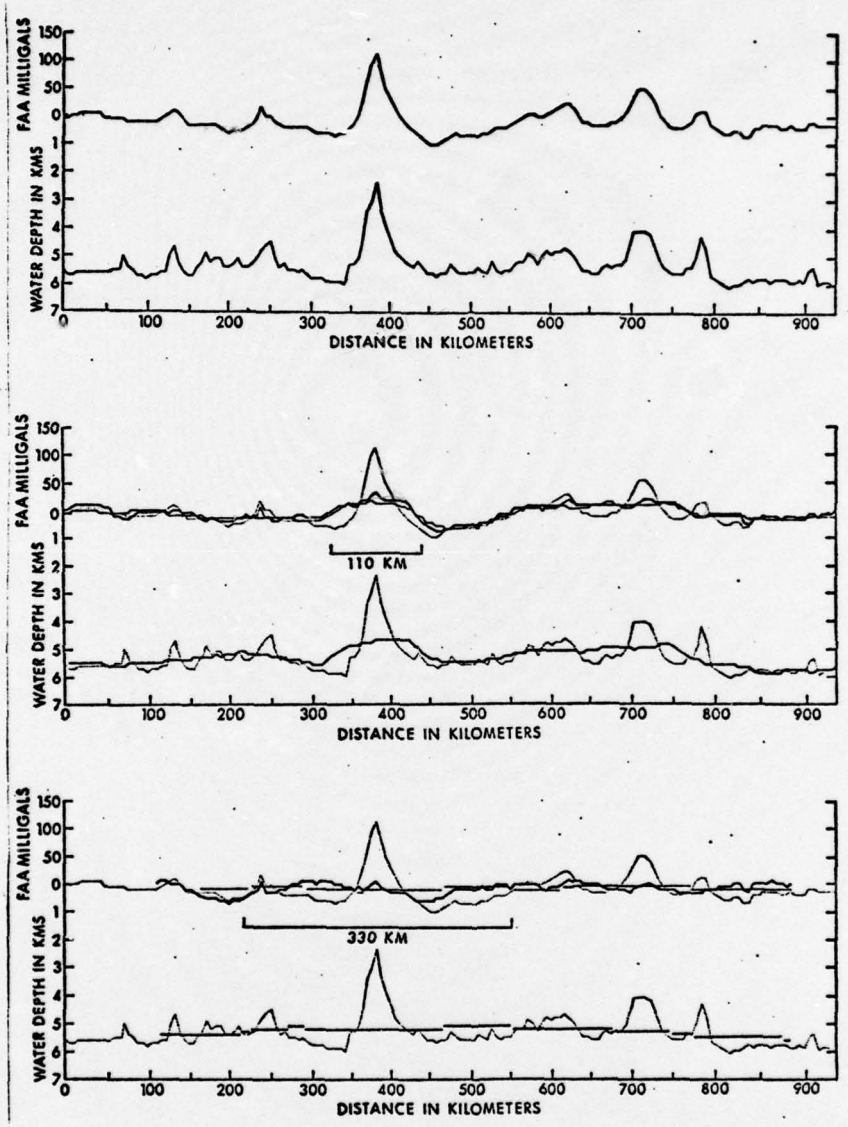

Figure 3. Profiles of the free-air anomaly and bottom topography used for a test of TCFAA. Original data are shown in (a). TCFAA (bold line) mean FAA (fine line), and mean bottom topography for a 110 km window are shown in (b). The same quantities as in (b) are shown in (c) for the case of a 330 km window.

CONCLUSIONS

1. Even in the worst case where a ship track crosses the axis of a submerged seamount, the 2D approximation for removal of bottom topography gravity effects is considerably better than use of a 1D flat-slab approximation.

2. Seamounts off to the side of the ship trackline and not seen by the echo-sounder can be effectively ignored as regards the correction of the free-air anomaly for their topographic effect.

3. The moving window TCFAA computer program with a 110 km window can be used very effectively for long ship tracks to give good 1°x1° free air anomaly approximations. In addition, the program is very useful for studying crustal structure problems when used with a 330 km window because the mean topography and mean free-air anomalies represent regional or "steady state" conditions while the TCFAA results represent local deeper structural gravity effects which are not contaminated or screened by the local topographic "noise-level."

4. The 330 km means should be very useful for setting up regional basic predictors.

5. The TCFAA program uses only what it can see, and suffers only from use of a 2D assumption. Therefore, it is in reasonable harmony with the principles of minimum astonishment.

APPENDIX A

THE VERTICAL GRAVITATIONAL ATTRACTION OF A HORIZONTAL CIRCULAR DISK

The vertical gravitational attraction of a very thin horizontal circular disk can be computed from the solid angle subtended by the disk. There are several different methods of calculating the solid angle, and the computational efficiency of each method varys with the horizontal as well as vertical distances from the disk.

The vertical gravitational attraction, g_z, of a horizontal disk is given by the volume integral

$$g_z = \int_V \frac{\gamma\delta\cos\theta}{r^2}\, dV \qquad (1)$$

where γ is the gravitational constant, δ is the density, r is the distance of the field point from the source point on the disk, and θ is the angle between r and the normal to the disk. This is shown in Figure A1.

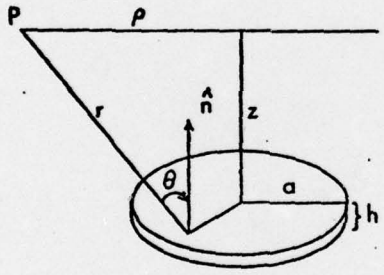

Figure A1. Diagram of vertical gravitional effect of a horizontal disk.

For $h \ll r$, (1) reduces to

$$g_z \approx \gamma\delta h \int_A \frac{\cos\theta}{r^2}\, dA \qquad (2)$$

where A represents the area of the disk. The solid angle at field point P subtended by the disk is

$$\Omega = \int_A \frac{\hat{n}\cdot\vec{dA}}{r^2} \qquad (3)$$

where $\hat{n}$ is the unit vector normal to the surface of the disk and $\vec{dA}$ is the element of area (dA) vector directed along the line of length r. Now (3) reduces to

$$\Omega = \int_A \frac{\cos\theta}{r^2}\, dA \qquad (4)$$

which is the same integral as the one in (2). Then (1) for a thin disk can be expressed as

$$g_z \approx \gamma\delta h\Omega \ . \tag{5}$$

The value of Ω on the axis (ρ=o) reduces to

$$\Omega_o = 2\pi\,(1-Z/\sqrt{Z^2+a^2}) . \tag{6}$$

The evaluation of the integral for a point off the axis is much more complicated. Some methods have used power series expansions, and others have determined closed form solutions in terms of Elliptic integrals of the first, second and third kinds.

Jaffey (1954) lists results of Zumwalt obtained by expanding the integrand in a binomial series and then integrating term by term. Since the integrand of (4), $\cos\theta/r^2$, is a solution of Laplace's equation, the solid angle can also be expressed in terms of a Legendre polynomial series of the form

$$\Omega = \sum_{n=o}^{\infty} A_n \left(\frac{a}{r}\right)^{n+1} P_n\,(\cos\theta), \quad r>a \tag{7a}$$

$$\Omega = \sum_{n=o}^{\infty} A_n \left(\frac{r}{a}\right)^{n} P_n\,(\cos\theta), \quad r<a \tag{7b}$$

where $\cos\theta = Z/\sqrt{Z^2+\rho^2}$
The coefficients A_n can be solved for by comparison with the terms of the Zumwalt expansion for the on-axis case.

Refer to Jeans (1958), p. 431, for an example of this procedure. The particular result most suitable for our purposes is

$$\Omega = -2\pi \sum_{n=1}^{\infty} P_{2n}\,(0)\; P_{2n-1}\,(\cos\theta)\; \left(\frac{a}{r}\right)^{2n}, \quad r>a \tag{8}$$
$$\text{(J-7b)}$$

which converges rapidly for r >> a. Other types of series expansion results are also given by Jaffey. We denote (8) as our Equation (J-7b) where prefix J refers to Jaffey.

Other approaches to the problem have provided exact solutions in terms of the complete and incomplete Elliptic integrals. One such solution is derived by Paxton (1959). Starting from (4) he obtains

$$\Omega = 2\int_{o}^{\beta max}\int_{o}^{\varphi_s} \sin\varphi\, d\varphi\, d\beta \ . \tag{9}$$

Refer to Figure A2. The line integral over φ is obtained first.

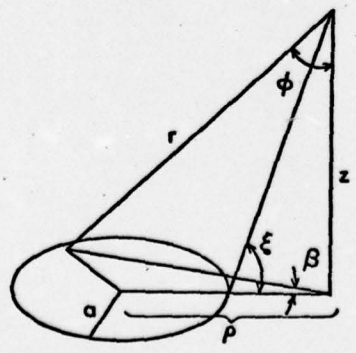

Figure A2. Quantities involved in Paxton's solution.

After expressing φ_s and β in terms of ξ and other parameters the resulting integrals become the complete elliptic integrals of the first and third kinds. To simplify the expression, the Elliptic integral of the third kind is expressed in terms of Heuman's lambda function, Λ_o. The following results were obtained by Paxton:

$$\Omega = 2\pi - \frac{2Z}{\sqrt{Z^2 + (\rho+a)^2}} K(k) - \pi\Lambda_o(\xi,k), \quad \rho<a \qquad (10a)$$

$$\Omega = \pi - \frac{2Z}{\sqrt{Z^2 + (\rho+a)^2}} K(k), \quad \rho=a \qquad (10b)$$

$$\Omega = \frac{-2Z}{\sqrt{Z^2 + (\rho+a)^2}} K(k) + \pi\Lambda_o(\xi,k), \quad \rho>a \qquad (10c)$$

where

$$k^2 = \frac{4\rho a}{Z^2 + (\rho+a)^2}\ ;\ \xi = \sin^{-1}\left[\frac{1-k^2/\alpha^2}{1-k^2}\right]^{1/2}\ ;\ \alpha^2 = \frac{4\rho a}{(\rho+a)^2}$$

and K(k) is the complete Elliptic integral of the first kind. The Heuman lambda function can be expressed in a series containing K(k), E(k) (the complete Elliptic integral of the second kind), ξ, and k. To evaluate Paxton's results, refer to Nagy (1965) as well as Abramowitz and Stegun (1970), chapter 17.

Another exact solution for Ω in terms of Elliptic integrals was obtained by Tallqvist and referred to by Garrett (1954). Tallqvist approximated the exact solution as

$$\Omega = 2\pi - 2\pi \sin\theta \left[1 - \tfrac{1}{4}k^2 - \tfrac{1}{64}k^4(3-4\tan^2\theta)\ldots\right] \qquad (11)$$

in this case $k^2 = (\rho^2+Z^2+a^2-S)/(\rho^2+Z^2+a^2+S)$, $S = [(\rho^2+Z^2-a^2)^2 + 4a^2Z^2]^{1/2}$, $\sin^2\theta = (\rho^2+Z^2-a^2+S)/2S$ and $\tan\theta = 2aZ/(S+a^2-\rho^2-Z^2)$.

The solutions given here, as well as some others, were examined to determine the best series to use in different regions to achieve a given accuracy with a minimum number of computations involved. The accuracy of Ω was arbitrarily set at 0.0001 radian for the test case. For each solution, Ω was computed term by term until the term was less than the desired accuracy. The resulting sum for each series was then compared with tabularized solid angle values (Masket, 1957, 1962) to confirm that the series had in fact converged. For computer applications, the regions adopted are shown in Figure A3 and indicate the particular equation used and the associated numbers of terms required to achieve an accuracy of 0.0001 radian. The scales for ρ and Z are not linear as the only purpose is to show the general regions.

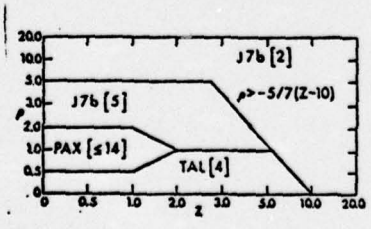

Figure A3. Regions of ρ and Z adopted for 0.0001 radian accuracy. Equation used and numbers of terms required are given, except that for the Paxton solution, 14 refers to the number of terms used in Heuman's lambda function.

ACKNOWLEDGEMENTS

The seamount studies, which had many details not reported here, as well as the Ω equation and associated computer program development, are the work of Bruce Bowman. The modifications to get pairs of (x, z) values along an off-axis flank crossing of a conical seamount, as well as the 2D-3D investigations and TCFAA are the work of J. C. Rose. The investigations were supported in part by Office of Naval Research contract N00014-70-A-0016-0001 and in part by National Science Foundation grant GX 28674 (IDOE Nazca Plate).

BIBLIOGRAPHY

Abramowitz, M., and I. Stegun. Handbook of Mathematical Functions with Formulas, Graphs, and Mathematical Tables, U.S.-Government Printing Office, Washington, D. C., 1970. (Chap. 17).

Byrd, P. F. and M. C. Friedman. Handbook of Elliptic Integrals for Engineers and Physicists, Springer-Verlag, Berlin, 1954.

Furumoto, A. S., J. F. Campbell and D. M. Hussong. Seismic refraction surveys along the Hawaiian Ridge, Kauai to Midway Island, Bulletin of the Seismological Society of America, 61, 147-166, 1971.

Garrett, M. W. Solid angle subtended by a circular aperture, Review of Scientific Instruments, 25 (12), 1954. (p. 1208).

Grosjean, C. C. Series expansions for the solid angle subtended by a circular disk at a point directly above the periphery, Rev. Sci. Instr., 38 (8), 1967. (p. 1042).

Jaffey, A. H. Solid angle subtended by a circular aperture at point and spread sources: Formulas and some tables, Rev. Sci. Instr., 25 (4), 1954. (p. 349).

Jeans, J. H. The Mathematical Theory of Electricity and Magnetism, Cambridge University Press, 1958. (p. 431).

Krause, D. C. Interpretation of echo sounding profiles, International Hydrographic Review, 39 (1), 5-123, 1962.

Ludwig, W. J., J. E. Nafe, and C. L. Drake. Seismic refraction, in the Sea, Vol. 4, part 1, edited by A. Maxwell, pp. 53-84, Interscience, N. Y., 1970.

Masket, A. V. Solid angle contour integrals, series, and tables, Rev. Sci. Instr., 28 (3), 1957. (p. 191).

Masket, A. V., and W. C. Rodgers. Tables of solid angles, U.S.A.E.C. Technical Report TID-14975 Physics, 1962.

Nagy, D. The evaluation of Heuman's Lambda Function and its application to calculate the gravitational effect of a right circular cylinder, Pure and Applied Geophysics, 62, (26) 1955.

Nettleton, L. L. Gravity and magnetic calculations, Geophysics, 7, 1942. (p. 293).

Parasnis, D. S. Exact expressions for the gravitational attraction of a circular lamina at all points of space and of a right circular vertical cylinder at points external to it, Geophysical Prospecting, 9 (3), 1961. (p. 382).

Paxton, F. Solid angle calculation for a circular disk, Rev. Sci. Instr., 30 (4), 1959, (p. 254).

Rapp, R. H. The geoid: Definition and determination, EOS, 55 (3), 118-126, 1974.

Reilly, W. Gravitational and magnetic effects of a right circular cylinder, New Zealand Journal of Geology and Geophysics, 12, 1969. (p. 497).

Strange, W. E., G. P. Woollard and J. C. Rose. An analysis of the gravity field over the Hawaiian Islands in terms of crustal structure, Pacific Science, 19, 381-389, 1965.

Talwani, M., J. L. Worzel and M. Landisman. Rapid gravity computations for two dimensional bodies with application to the Mendocino submarine fracture zone, Jour. Geophys. Res., 64, 49-59, 1959.

Woollard, G. P. A gravity reconnaissance of the island of Oahu, Trans. Am. Geophys. Union, 32, 358-368, 1951.

Woollard, G. P. The relation of gravity anomalies to surface elevation, crustal structure, and geology, Research Report 62-9, AF23(601)-3455, University of Wisconsin, 1962.

Woollard, G. P. Collection, processing, and geophysical analysis of gravity and magnetic data, Final Report to AF Contract F23(601)-67-C-0168, Hawaii Institute of Geophysics, 1968.

Hawaii Institute of Geophysics Contribution No. 608.